PHOTOCATALYTIC ACTIVITY OF DEFECTIVE TIO$_{2-X}$ FOR WATER TREATMENT/METHYL ORANGE DYE DEGRADATION

Safaa H. Ali[1, ✉], Saad S. Mohammed[2], Mohsin E. Al-Dokheily[2], Laith Algharagholy[3]

Abstract. This study is designed to highlight photocatalytic activity of TiO$_2$ nanoparticles in methyl orange (MO) dye degradation. Titanium dioxide TiO$_2$ nanopowder was synthesized by conventional sol-gel method and calcined in air atmosphere at different temperatures 350°C, 550°C and 850°C. The prepared TiO$_2$ nanoparticles then were subjected to a solid state reaction with calcium hydride (CaH$_2$) at the same temperatures but calcined in argon atmosphere. X-Ray Diffraction (XRD) measurements used for phase and crystalline size identification showed that the obtained samples have the same TiO$_2$ anatase phase, but the crystalline size decreased after reduction treatment. The electronic properties obtained *via* UV spectroscopy showed the decrease in calculated energy gap from 3.3 eV for prepared TiO$_2$-550 to 2.65 eV for reduced TiO$_2$-CaH2-550, which extend the absorption spectra toward visible light region. Energy dispersive spectroscopy (EDS) and scanning electron microscope (SEM) measurements revealed that the particle size decreased after reduction treatment similar to the XRD crystalline size. EDS results indicated that the deficient in oxygen content relates to formation oxygen vacancies responsible for nonstoichiometric TiO$_{2-x}$ oxides formation. The synthesized reduced TiO$_2$ showed an excellent photo-catalytic activity in methyl orange dye degradation under optimum condition: pH 4.5, 40 mg catalyst loading and 10 ppm initial dye concentration.

Keywords: CaH$_2$, photocatalytic activity, oxygen vacancy, solid state, TiO$_2$.

[1] Department of Physiology and Chemistry, College of Veterinary Medicine, University of Thi-Qar, Al-Shatrah, Thi-Qar, Iraq, 64007
[2] Department of Chemistry, College of Science, University of Thi-Qar, Al-Nasriyah, Thi-Qar, Iraq, 64002
[3] Department of Physics, College of Science, University of Sumer, Al-Refaie, Thi-Qar, Iraq
✉ *safaa.ali@utq.edu.iq*

1. Introduction

Nanoparticles of TiO$_2$ have a wide range of applications in the environmental and energy fields, including wastewater treatment, hydrogen evolution, photo electrochemical conversion and sterilization.[1,2] Photocatalysis represents one of the most commonly used method for water treatment, which uses a catalyst to accelerate the photo-reaction.[3] The photon absorption ability of the catalyst from light induces the generation of electron-hole pairs in the photo-reaction process. The created electron at the conduction band (CB) of the catalyst is used for reduction reaction. Also, the catalyst holes at the valence band (VB) can be used for the oxidation reaction. A photocatalytic process is extensively used to produce hydrogen and oxygen *via* water splitting,[4] degradation of dye[5] and reduction of CO$_2$.[6] One of the widely used photocatalysts in the photocatalytic process is titanium dioxide (TiO$_2$). This is related to its chemical stability, low cost, availability, and resistance to corrosion. However, the use of TiO$_2$ as a photocatalyst is subjected to some limitations. The wide band gap of TiO$_2$ makes it active under UV light irradiation, therefore it is not effective under sunlight, which consists of only about 4 % UV light from the solar spectrum. Moreover, the high rate of recombination process compared to chemical interaction rate with the adsorbed species required for redox reactions.[7] While, the defects in TiO$_2$ including bulk oxygen vacancies, surface oxygen vacancies and Ti^{3+} can prevent the recombination of photo-generated charges by a trapping electron.[8] The Ti^{3+} and surface oxygen vacancies are generated together because one oxygen atom deficient at bridging O site creates two surface Ti^{3+} exposed sites.[9] Incorporation of surface oxygen vacancies and Ti^{3+} in TiO$_2$ can be conducted using different ways such as annealing TiO$_2$ under reduction condition or vacuum atmosphere,[10] high energy particle bombardment,[11] and UV irradiation.[12]

In this work, we used solid state reduction reaction to prepare reduced TiO$_2$ nanoparticles with oxygen vacancies defects. The reduced TiO$_2$ nanoparticles sho-

wed a good photocatalytic activity in methyl orange dye degradation as compared with prepared TiO_2.

2. Experimental

2.1. Chemical Materials

All chemicals used in this study (titanium tetraisopropoxide TTIP 97 %, calcium hydride 99.99 %, 2-propanol 95.5 %, nitric acid 90 %, methyl orange dye 99.5 %) were purchased from Sigma-Aldrich and used as received.

2.2. Synthesis of TiO_2 Nanoparticles

TiO_2 nanoparticles were prepared *via* the sol-gel method using titanium tetraisopropoxide (TTIP), 2-propanol, and deionized water.[13] 2-Propanol was mixed with deionized water in weight ratio (2-propanol : TTIP : H_2O = = 1 : 2 : 12) and was added dropwise to TTIP solution under continuous stirring. After that the aqueous solution was acidified with nitric acid (pH = 2.0) and kept under stirring overnight. A suspension solution was formed and the solution was separated into two layers. The upper layer was the organic by-product of the hydrolysis and the titanic acid gel occupied the lower layer of the solution mixture. The precipitate gel was filtrated and dried in an oven at 110°C overnight. Dry block yellow crystals were ground into fine powder and the sample was assigned as TiO_2-110. Further calcination at (350, 550 and 850°C) has been done for 4 h and the prepared TiO_2 was assigned as TiO_2-350, TiO_2-550 and TiO_2-850, respectively.

2.3. Synthesis of Reduced TiO_2 Nanoparticles

Solid state reactions were used to prepare reduced TiO_2 nanoparticles. 1 mole of prepared TiO_2 nanoparticles was mixed carefully with 1 mole of CaH_2, the mixture was grounded thoroughly and placed in a quartz tube furnace. Argon gas (99.99 %) was used as an atmosphere with steady flow rate of 50 cm^3/min. The temperature in the tube furnace was rapidly raised up to 350, 550 and 850 °C, the process continued for four hours and then the furnace was turned off to cool down. Finally, the product was carefully collected and washed with deionized water and methanol several times to remove unreacted reducing agent. The resulted nanoparticles were assigned as TiO_2-CaH_2-350, TiO_2-CaH_2-550 and TiO_2-CaH_2-850.

2.4. Characterization

Analytical Philips diffractometer (Cu target Ka radiation, λ = 1.541 Å) was used to measure the phase and crystalline size. The XRD data were collected at 2θ (10° to 80°). Scanning Electron Microscope (als2300 Angstrom) was used to get SEM images of the samples by employing a high-energy beam of electrons. Energy dispersive X-ray spectrometer (EDS) was combined with SEM to investigate the composition of the samples. The band gap energies of the prepared and reduced TiO_2 were measured by diffuse reflectance spectra using an UV–VIS spectrophotometer. The UV–VIS spectra were collected for the dry pressed disk samples equipped with an integrating sphere assembly, and $BaSO_4$ as a reflectance reference. Surface area of the samples was determined by micromeritics Auto Chem Chemisorption analyzer depending on nitrogen adsorption/desorption isotherm.

2.5. Photocatalytic Activity Measurements

Photochemical immersion reactor equipped with medium pressure Mercury Lamp 400W MVL41-SAIC was used in this work to perform the photocatalytic experiments. Methyl orange (100 mL) solution was used in the photoreactor for photocatalytic activity measurements. A mixture of dye solution and the photocatalyst was stirred in the dark (20 min) to reach the adsorption equilibrium on the photocatalyst surface, and then the solution was irradiated. The mixture solution was filtrated at different time intervals to collect the photocatalyst particles, then centrifuged for 10 min and finally filtered by cellulose membrane (0.45 μm). The absorbance of MO dye was measured by UV–Vis spectrophotometer at 465 nm to determine the degradation percent. The degradation efficiency of the MO dye percentage was calculated according to the equation below:

Degradation efficiency, % = $[1 - (C_t/C_0)] \cdot 100$ %   (1)
where C_t is the concentration after time t and C_0 is the initial concentration of the dye.

3. Results and Discussion

3.1. Phase and Crystalline Size Features

X-ray (XRD) analysis has been performed for prepared and reduced TiO_2. The XRD patterns of the prepared TiO_2 at 350 °C, 550 °C and 850 °C are shown in Fig. 1. The diffraction signals for TiO_2 anatase phase were clearly observed for calcined samples at 350°C and 550 °C (JCPDS Card No. 00-021-1272), while TiO_2 rutile phase signals were recorded for calcined samples at 850 °C (JCPDS Card No. 00-021-1276). The XRD peak located at 2θ = 25.28° often represents the characteristic peak of TiO_2 anatase (101) plane. The signals related to the anatase (101) appeared at 2θ = 25.16° and 25.54° for

TiO$_2$-350 and TiO$_2$-550, respectively (Table 1). For TiO$_2$-850 sample, the characteristic signal appeared at 2θ = 27.32° related to TiO$_2$ rutile phase.

As illustrated in Fig. 2 and Table 1, the characteristic peak signal of samples reduced with CaH$_2$ at 350 °C and 550 °C shifted toward higher values and appeared at 2θ = 25.36° and 25.74° for TiO$_2$-CaH$_2$-350 and TiO$_2$-CaH$_2$-550, respectively. Similarly, for the TiO$_2$ sample reduced at 850 °C the characteristic peak signal showed higher 2θ value and appeared at 27.52° for TiO$_2$-CaH$_2$-850.

However, at 2θ values approximately all reduced samples at different temperatures showed a noticeable shifting and peaks broadening to higher values due to the formation of oxygen vacancies.[14] Scherrer equation was employed to calculate the mean crystallite sizes (D) by using XRD data.[15]

$$D = \frac{K\lambda}{\beta\cos\theta}, \qquad (2)$$

where D is the mean crystallite size in nm, λ is wavelength of the X-ray radiation (0.15405 nm for Cu kα), K is the Scherrer constant (0.89) which depends on the shape of the crystal, β is the full width of half-maximum (FWHM) intensity.

Table 1 shows the crystallites size were 11.82 nm, 16.29 nm and 16.86 nm for TiO$_2$-350, TiO$_2$-550 and TiO$_2$-850, respectively. After reduction treatment the crystallites size of TiO$_2$ decreased to 11.15 nm, 14.69 nm and 16.42 nm for TiO$_2$-CaH$_2$-350, TiO$_2$-CaH$_2$-550 and TiO$_2$-CaH$_2$-850, respectively.
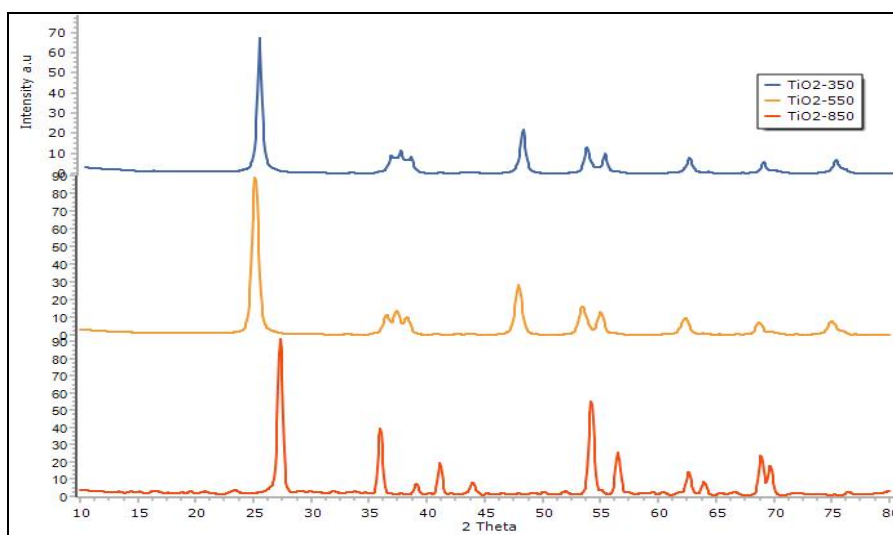
Fig. 1. XRD patterns of the as prepared TiO$_2$ at 350°C, 550°C and 850°C
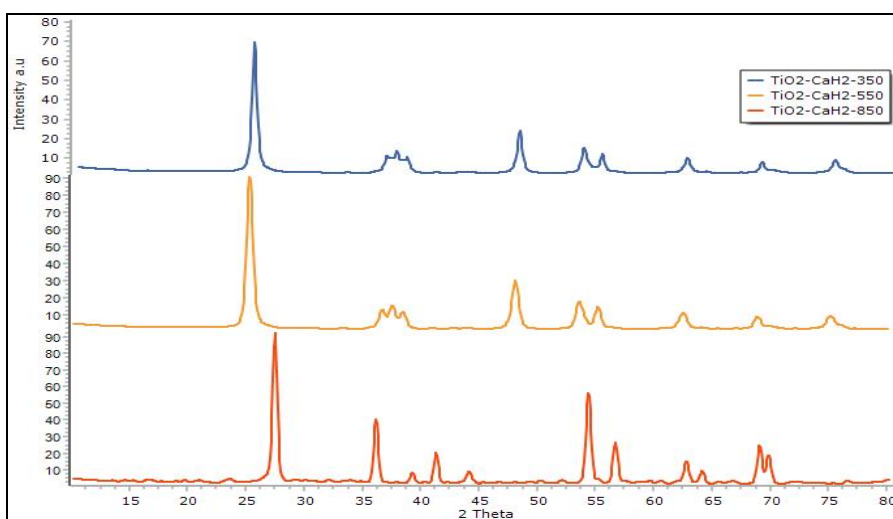
Fig. 2. XRD patterns of the reduced TiO$_2$ at 350°C, 550°C and 850°C

Table 1. XRD patterns data and mean crystallite size (*D*) for prepared and reduced TiO$_2$

Sample	Phase	Miller indices (*h k l*)	2θ (°)	FWHM (°)	*D* (nm)
TiO$_2$-350	Anatase	1 0 1	25.16	0.650	
	Anatase	2 0 0	48.01	0.696	
	Anatase	1 0 5	53.44	0.819	11.82
TiO$_2$-550	Anatase	1 0 1	25.540	25.540	
	Anatase	2 0 0	48.310	48.310	
	Anatase	1 0 5	53.840	53.840	16.29
TiO$_2$-850	Anatase	1 1 0	27.32	0.497	
	Anatase	1 0 1	36.04	0.472	
	Anatase	2 1 1	54.22	0.525	16.86
TiO$_2$-CaH$_2$-350	Anatase	1 0 1	25.36	0.662	
	Anatase	2 0 0	48.16	0.735	
	Anatase	1 0 5	53.64	0.917	11.15
TiO$_2$-CaH$_2$-550	Anatase	1 0 1	25.740	0.478	
	Anatase	2 0 0	48.540	0.557	
	Anatase	1 0 5	53.860	0.749	14.69
TiO$_2$-CaH$_2$-850	Rutile	1 1 0	27.52	0.501	
	Rutile	1 0 1	36.18	0.500	
	Rutile	2 1 1	54.42	0.532	16.42

Table 2. Lattice parameters for prepared and reduced TiO$_2$ at 350°C, 550°C and 850°C

Sample	Cell parameters (*a*, *b*) Å	Cell parameter (*c*) Å	Cell volume Å^3
TiO$_2$-350	3.786	9.894	141.81
TiO$_2$-CaH$_2$-350	3.774	9.532	135.76
TiO$_2$-550	3.764	9.205	130.41
TiO$_2$-CaH$_2$-550	3.746	8.993	126.19
TiO$_2$-850	4.611	2.958	62.89
TiO$_2$-CaH$_2$-850	4.579	2.950	61.85

However, the reduction treatment was not the only factor that affected the crystallite size; the another factor was temperature and the samples reduced at high temperature had large crystallite size as compared with samples reduced under low temperature.[16] The lattice parameters (*a* and *c*) collected from the XRD data using Bragg's law by the relation applied for the tetragonal crystal symmetry as given below.[17]

$$(1/d^2_{hkl})=[(h^2+k^2+l^2)/a^2]+(l^2/c^2) \qquad (3)$$

where *h*, *k* and *l* is Miller indices while *d$_{hkl}$* is the inter planar spacing of the crystal lattice.

The standard values of lattice parameters and cell volume of anatase TiO$_2$ (JCPDS Card No. 00-021-1272) are: *a* = 3.7852 Å, *c* = 9.5139 Å and Cell Volume = 136.31 Å^3; for rutile TiO$_2$ (JCPDS Card No. 00-021-1276) *a* = 4.5933 Å, *c* = 2.9592 Å and Cell Volume = 62.43 Å^3.

The calculated lattice parameters and cell volume are shown in Table 2; there is a good agreement between the calculated lattice parameters and cell volume with standard values for anatase and rutile TiO$_2$. However, a significant decrease in lattice parameters and cell volume was observed after reduction treatment, as a result of

oxygen vacancies formation. This slightly reduces the crystallite size and induces lattice contraction.[18]

3.2. UV−VIS Diffused Reflectance Spectra

The optical properties of the TiO$_2$ nanoparticles were characterized by UV–Vis diffuse reflectance spectra (DRS). The absorption spectra are shown in Figs. 3 and 4. The DRS spectra show that the absorption edge is around 370 nm, 375 nm and 430 nm for prepared TiO$_2$-350, TiO$_2$-550 and TiO$_2$-850, respectively. However, the reduced TiO$_2$ samples absorb at longer wavelengths and the absorption edges are around 450 nm, 467 nm and 501 nm for TiO$_2$-CaH$_2$-350, TiO$_2$-CaH$_2$-550 and TiO$_2$-CaH$_2$-850, respectively. This means that all reduced TiO$_2$ samples absorb in the visible light region compared to the prepared samples, which absorb mainly in the ultraviolet region.

To more understand the optical properties, the energy gaps (*E$_g$*) were calculated for all TiO$_2$ samples at different temperatures using Tauc plot, according to the following equation.[19]

$$\alpha h v = A(h v - E_g)^{1/2} \qquad (4)$$

where α is the absorption coefficient, A is the constant. E_g values calculated by using extrapolating the tangent line of the $(\alpha h v)^{1/2}$ plot drown *vs. hv.*

The Tauc plots are shown in Figs. 5 and 6 and the calculated energy gaps are listed in Table 3. The energy gap values are 3.35 eV, 3.3 eV and 2.88 eV for TiO$_2$-350, TiO$_2$-550 and TiO$_2$-850, respectively. As compared with the prepared TiO$_2$, all reduced TiO$_2$ nanoparticles show notable decrease in the energy gaps which take the following values: 2.7 eV, 2.65 eV and 2.4 eV for TiO$_2$-CaH$_2$-350, TiO$_2$-CaH$_2$-550 and TiO$_2$-CaH$_2$-850, respectively. Because of the wide energy gap of TiO$_2$, it can absorb only the UV light; if one oxygen atom is lost during the reduction process, the optical properties of TiO$_2$ can be modulated by introducing oxygen vacancies and advancing the TiO$_2$ absorption from UV to the visible light region. Local states are below the conduction band minimum as a result of oxygen vacancies formation and these new vacancy states could contribute to a new photoexcitation process. As the electrons in the valence band can be excited to the oxygen vacancy states with the energy of visible light, this leads to a typical excitation in the visible light region of the spectrum.[20] In addition, the electrons lifted in the oxygen vacancies can be interacted with adjacent Ti^{4+} to produce the Ti^{3+} defect species. As a result, shallow donor levels for Ti^{+3} defect are formed below the conduction band, which also attributes to absorption of visible light.[21]
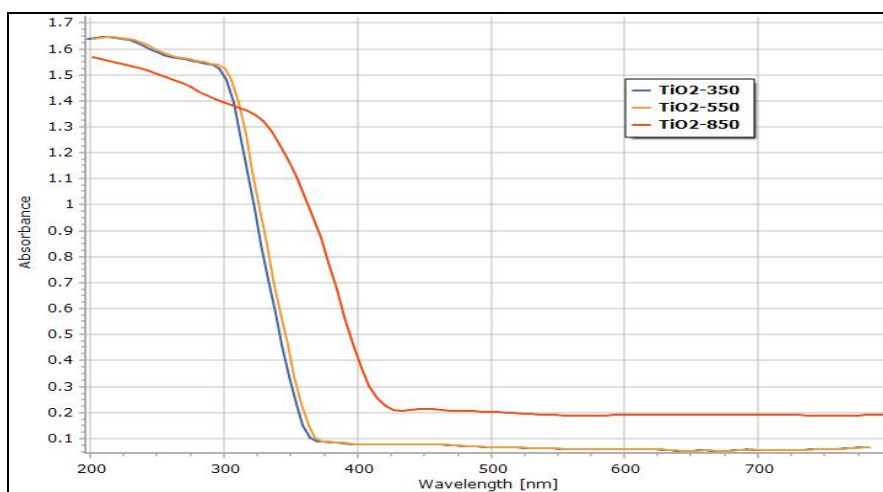
Fig. 3. DRS spectra of prepared TiO$_2$ at 350°C, 550°C and 850°C
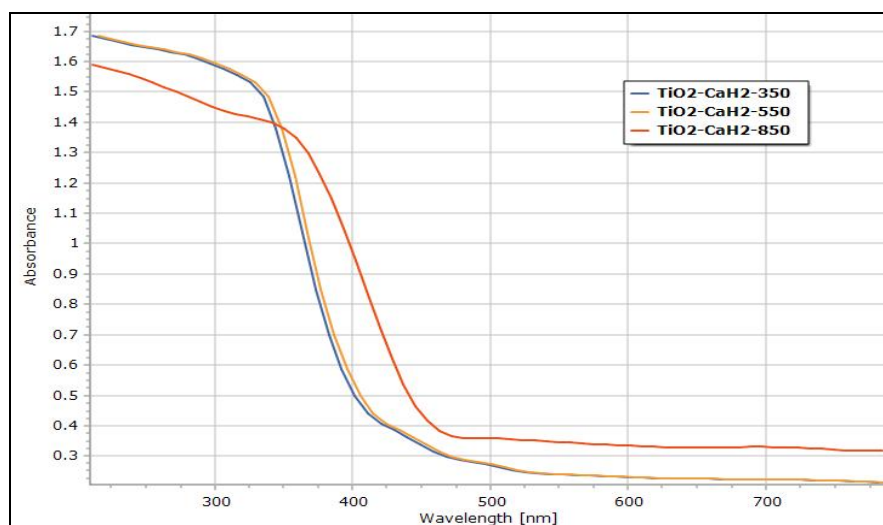
Fig. 4. DRS spectra of reduced TiO$_2$ at 350°C, 550°C and 850°C
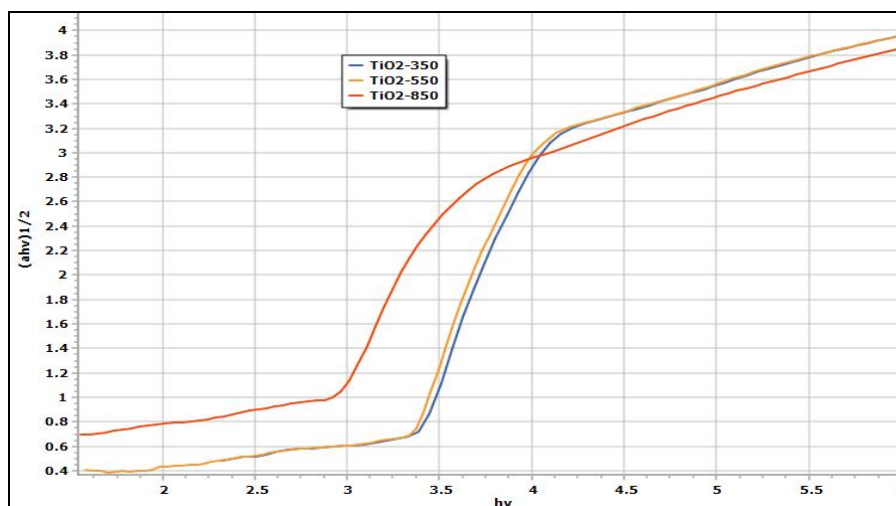
Fig. 5. Tauc plot for as prepared TiO_2 at 350°C, 550°C and 850°C
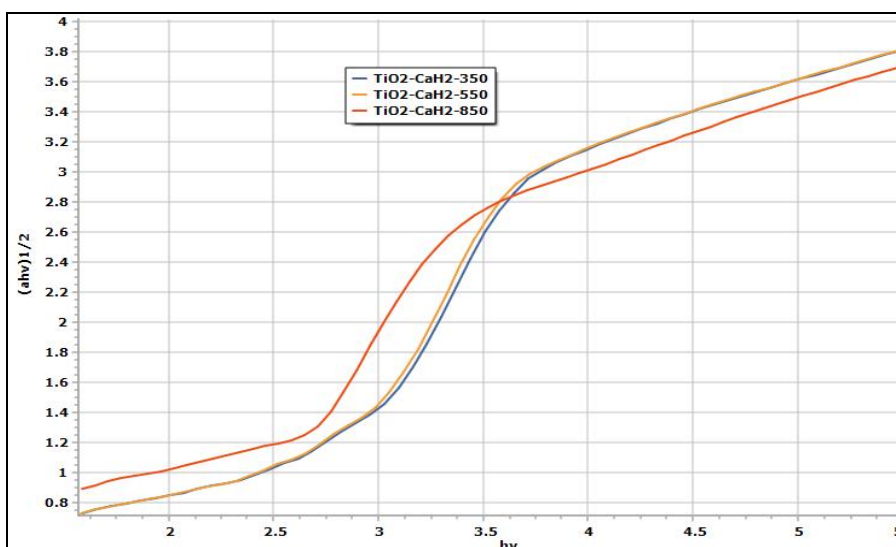
Fig. 6. Tauc plot for reduced TiO_2 at 350°C, 550°C and 850°C

Table 3. Calculated energy gaps (eV)

Sample	Energy gap (eV)
TiO_2-350	3.35
TiO_2-CaH_2-350	2.7
TiO_2-550	3.3
TiO_2-CaH_2-550	2.65
TiO_2-850	2.88
TiO_2-CaH_2-850	2.47

3.3. Scanning Electron Microscope (SEM) Coupled with Energy Dispersive Spectroscopy (EDS)

Surface morphological properties of prepared and reduced TiO_2 nanoparticles are characterized by scanning electron microscope (SEM); the resulted images are given in Fig. 7. High dispersive, spherical aggregated nanoparticles have been observed for all samples before and after reduction treatment; this indicates there is no morphology change and after the reduction treatment the particles have the same shape. However, the important change was noticed for the mean particle sizes (D), which clearly decreased after reduction treatment. As illustrated in Table 4, the mean particle size of TiO_2-350, TiO_2-550 and TiO_2-850 are 64 nm, 84 nm and 118 nm, respectively. These values gradually decreased after reduction treatment and obtained values were 61 nm, 72 nm and 95 nm for TiO_2-CaH_2-350, TiO_2-CaH_2-550 and TiO_2-CaH_2-850, respectively. On the other hand, as the oxygen vacancies concentration increased, the particle size of reduced TiO_2 nanoparticles decreased.[22]
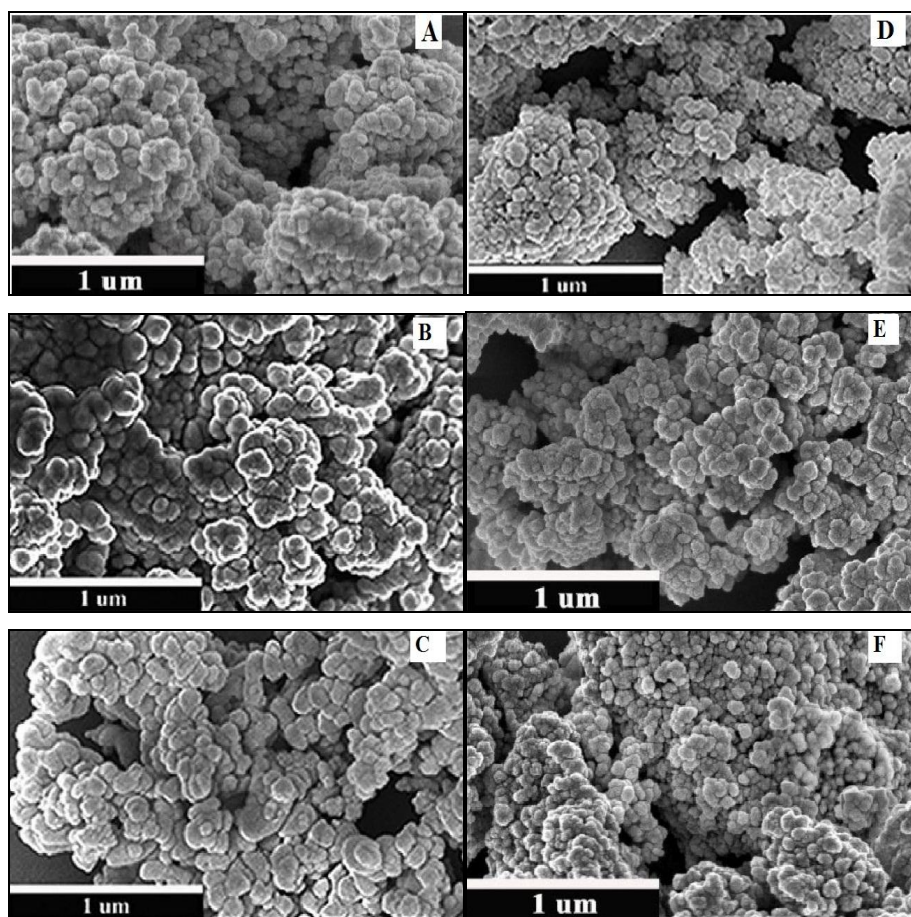
Fig. 7. SEM images of TiO$_2$-350 (A); TiO$_2$-550 (B); TiO$_2$-850 (C); TiO$_2$-CaH$_2$-350 (D); TiO$_2$-CaH$_2$-550 (E); TiO$_2$-CaH$_2$-850 (F)

Also, TiO$_2$ samples treated at 850 °C possess a larger particle size as compared with samples treated at 350 °C and 550 °C, which is attributed to the effect of temperature.[23] As compared with XRD crystallite size, the mean particle size has larger value; this difference is attributed to the polycrystalline nature of TiO$_2$ nanoparticles.[24]

Table 4. Mean particles size (*D*) obtained from SEM measurements

Sample	*D* (nm)
TiO$_2$-350	64
TiO$_2$-CaH$_2$-350	61
TiO$_2$-550	84
TiO$_2$-CaH$_2$-550	72
TiO$_2$-850	118
TiO$_2$-CaH$_2$-850	95

Energy dispersive X-ray spectroscopy (EDS) combined with SEM was used to investigate the elemental composition of TiO$_2$ samples; the obtained spectrums are shown in Fig. 8. These spectra clearly show only Ti and O peaks in EDS spectra. Thus, the experimental results prove the purity of the prepared and modified TiO$_2$ nanoparticles. Also, the atomic and weight ratios (insets in Fig. 8) confirm the above results about the purity of all samples.

However, the atomic and weight percentages (Fig. 8) can be used to estimate the stoichiometry and oxide formula for the resulted TiO$_2$ samples. One can see from Table 5 a significant deviation from the stoichiometry for the reduced TiO$_2$; the (O/Ti) ratio of TiO$_2$ before the reduction treatment is close to typical ratio (2 : 1). As the reduction treatment was performed, the deviation from stoichiometry tendency increased and the oxides of TiO$_{2-x}$ formula were formed. However, the relatively small amount of oxygen element in reduced TiO$_2$ indicate that more oxygen vacancies were created.[25]
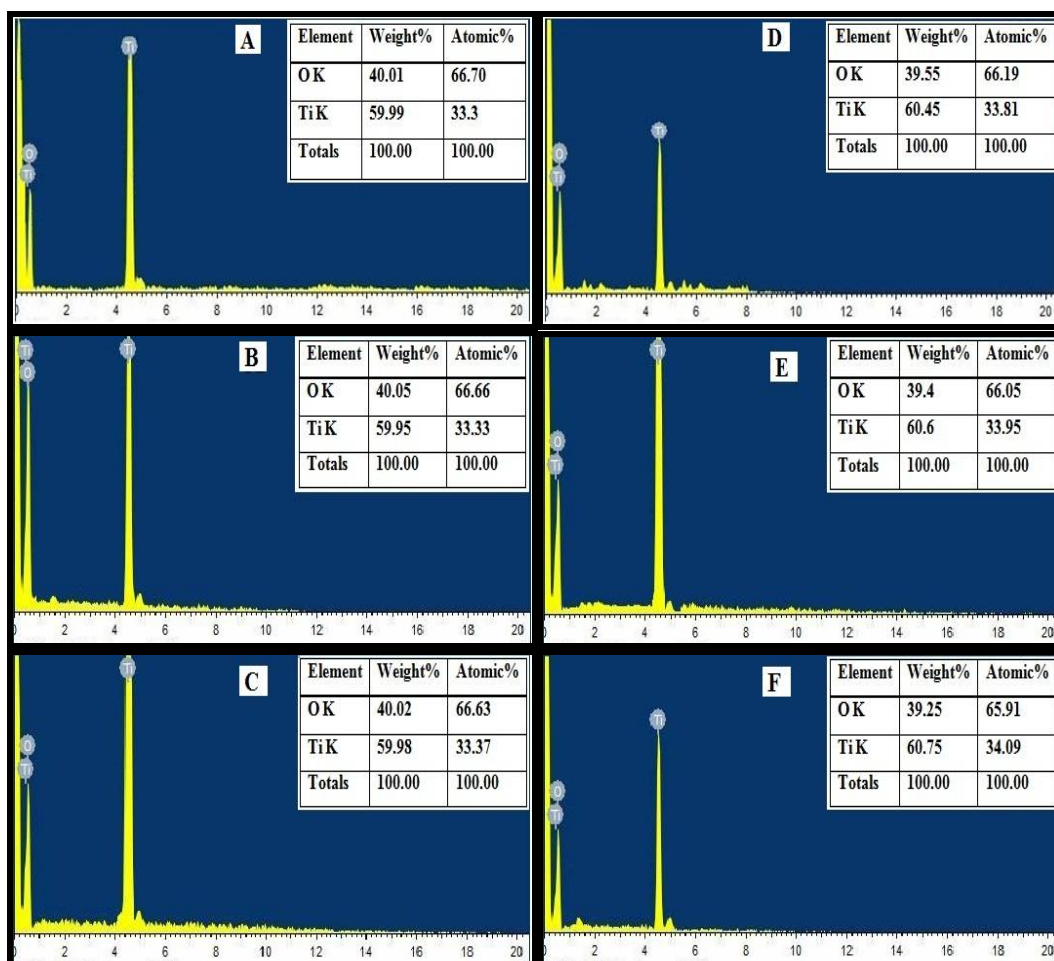
Fig. 8. EDS spectrums of TiO_2-350 (A); TiO_2-550 (B); TiO_2-850 (C); TiO_2-CaH_2-350 (D); TiO_2-CaH_2-550 (E); TiO_2-CaH_2-850 (F); insets represent the elemental weight and atomic percentage

Table 5. Oxides formulas calculated from EDS weight percentage

Sample	Oxide formula
TiO_2-350	TiO_2
TiO_2-CaH_2-350	$TiO_{1.957}$
TiO_2-550	TiO_2
TiO_2-CaH_2-550	$TiO_{1.945}$
TiO_2-850	$TiO_{1.996}$
TiO_2-CaH_2-850	$TiO_{1.933}$

3.4. Photocatalytic Activity and Factors Affecting MO Dye Photodegradation

3.4.1. Effect of Catalyst Loading

To study the impact of TiO_2 catalyst loading on the photodegradation of MO dye, different amounts (10–70 mg) of TiO_2 were used at pH = 4.5 and MO dye concentration of 10 ppm. The effect of TiO_2 dosages on degradation is shown in Figs. 9-11. The percent of degra-

dation of MO dye increases with increasing TiO_2 amount till 40 mg and then decreases. A sufficient catalyst amount can supply an adequate number of active sites, which means the increase in electron-hole pairs concentration and enhanced percent of degradation. However, the decrease in photocatalytic activity is observed at high catalyst loading related to the recombination of electron-hole pairs on the TiO_2surface.26 As shown in Fig. 12, under different catalyst loadings the photodegradation rate constant of MO dye reaches the maximum value under 40 mg catalyst loading in a similar trend with photodegradation percent. However, a significant difference in the rate constants of the same catalysts prepared at different temperatures was recorded; the rate constants at 40 mg catalyst dosage were 0.027, 0.041 and 0.026 K-1 for TiO_2-CaH_2-350, TiO_2-CaH_2-550 and TiO_2-CaH_2-850, respectively (Table 6TiO_2-CaH_2-550 exhibits larger degradation rate constant than TiO_2-CaH_2-850, despite the latter has a smaller energy gap. The best explanation is that the

TiO$_2$-CaH$_2$-850 nanoparticles exhibit rutile phase, the lower photocatalytic activity of rutile TiO$_2$ belongs to its fast electron-hole recombination, intrinsic defects, low specific surface area, and the location of conduction band minimum.[27] Also, the TiO$_2$-CaH$_2$-550 shows a higher catalytic activity than TiO$_2$-CaH$_2$-350, despite the latter has a larger surface area. This can be related to the increase in oxygen vacancies content in TiO$_2$ reduced at 550 °C if compared with the sample reduced at 350°C, as demonstrated by EDS measurements. The electron donor's property of oxygen vacancies in reduced TiO$_2$ improves charge transport and shifts the Fermi level of TiO$_2$ toward the conduction band, as well as accelerates the charge isolation.[28,29] Thus, photocatalytic activity of TiO$_2$-CaH$_2$-550 is better to compare with TiO$_2$-CaH$_2$-350.

Fig. 12. Effect of TiO$_2$ loading
on the degradation rate of MO
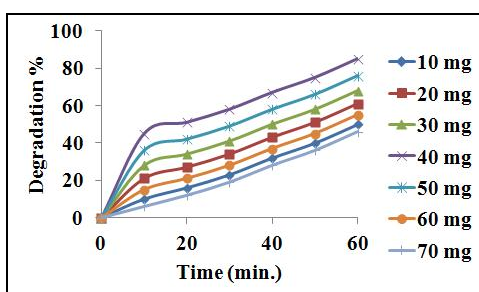
Fig. 9. Effect of TiO$_2$-CaH$_2$-350 dosage
on the degradation % of MO at pH = 4.5
and initial MO conc. 10 ppm
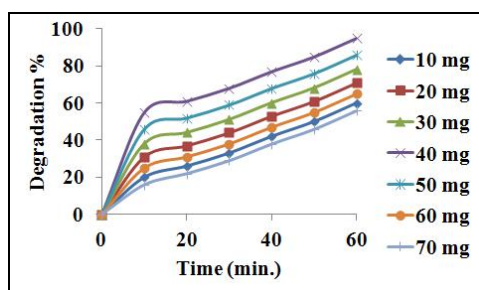
Fig. 10. Effect of TiO$_2$-CaH$_2$-550 dosage
on the degradation % of MO at pH = 4.5
and initial MO conc. 10 ppm
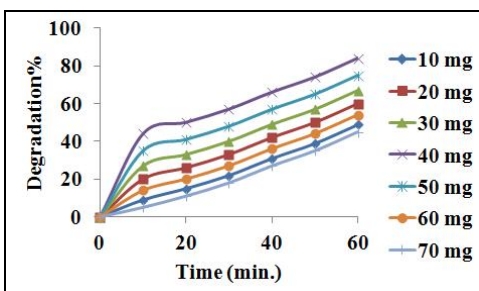
Fig. 11. Effect of TiO$_2$-CaH$_2$-850 dosage on the degradation %
of MO at pH = 4.5 and initial MO conc. 10 ppm

3.4.2. Effect of Initial pH

The impact of pH on the photodegradation of MO was carried out at different pH levels (4.5, 7.1, and 9). The pH was adjusted using H$_2$SO$_4$ and NaOH for the acidic and alkaline solutions respectively. The initial MO dye concentration was 10 ppm and the catalyst dosages 40 mg. Figs. 13-15 illustrate the pH effect on the photodegradation efficiency of MO dye; it is clearly observed that the photodegradation percent decreases with the increase in pH value, and the highest degradation efficiency was recorded at pH 4.5. According to the results represented in Table 7, it can be demonstrated that the photocatalytic efficiency at pH 4.5 after 60 min irradiation was 85 %, 95 % and 84 % for TiO$_2$-CaH$_2$-350, TiO$_2$- CaH$_2$-550 and TiO$_2$-CaH$_2$-850, respectively. However, the surface charge of the photocatalyst and the ionic nature of the dye (cationic or anionic) represent the key factors, which play an important role in the pH effect on the photodegradation process.[30] The adsorption of MO dye onto the TiO$_2$ surface is changed at different pH values; the point of zero charge (pzc) of TiO$_2$ is around pH 6.2.[31] In the acidic solution, the TiO$_2$ catalysts are positively charged at pH < 6.2; so, the electrostatic attraction of the negatively charged MO dye with positively charged TiO$_2$ creates a strong adsorption between the MO dye and the TiO$_2$ catalyst. At alkaline pH levels the process is inversed because of the Columbic repulsion of negatively charged TiO$_2$ with negatively charged MO dye, which decreases the adsorption of dye molecules on the surface of TiO$_2$ catalyst and finally decreases the photocatalytic activity.
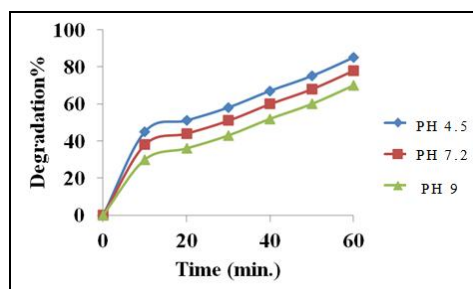
Fig. 13. Impact of initial pH on the percent of MO
photodegradation with TiO$_2$-CaH$_2$-350
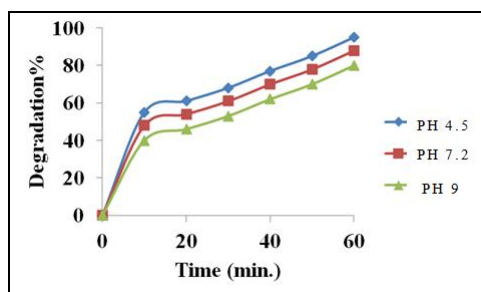
Fig. 14. Impact of initial pH on the percent of MO
photodegradation with TiO_2-CaH_2-550
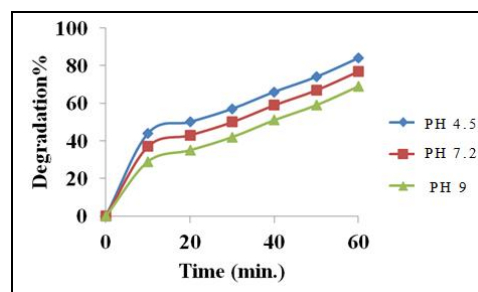
Fig.15. Impact of initial pH on the percent of MO
photodegradation with TiO_2-CaH_2-850

Table 6. Rate constants values for MO degradation different catalysts dosages

Catalyst	TiO_2-CaH_2-550						
Rate constant (min^{-1})	0.014	0.018	0.022	0.041	0.028	0.015	0.012
Dosage (mg)	10	20	30	40	50	60	70
Catalyst	TiO_2-CaH_2-350						
Rate constant (min^{-1})	0.011	0.014	0.017	0.027	0.020	0.012	0.010
Dosage (mg)	10	20	30	40	50	60	70
Catalyst	TiO_2-CaH_2-850						
Rate constant (min^{-1})	0.010	0.014	0.016	0.026	0.020	0.012	0.009
Dosage (mg)	10	20	30	40	50	60	70

Table 7. Photodegradation percentage of MO with different pH values

Time (min)	pH 4.5	pH 7.1	pH 9	pH 4.5	pH 7.1	pH 9	pH 4.5	pH 7.1	pH 9
	TiO_2-CaH_2-550			TiO_2-CaH_2-350			TiO_2-CaH_2-850		
	Deg. %			Deg. %			Deg. %		
0	0	0	0	0	0	0	0	0	0
10	55	48	40	45	38	30	44	37	29
20	61	54	46	51	44	36	50	43	35
30	68	61	53	58	51	43	57	50	42
40	77	70	62	67	60	52	66	59	51
50	85	78	70	75	68	60	74	67	59
60	95	88	80	85	78	70	84	77	69

3.4.3. Effect of OG Initial Concentration

To determine the impact of the MO dye concent-
ration on the photodegradation process different concent-
rations (5, 10, 15, 20, 25, 30 ppm) were studied. The plots
between ln C_o/C_t and the irradiation time are shown in
Figs. 16-18 and the calculated rate constants and the
degradation percents are summarized in Table 8. Accor-
ding to these results, the optimum MO concentration
responsible for the high degradation percent is 10 ppm for
all TiO_2 catalysts; the degradation percents at 10 ppm MO
concentration were 85, 95 and 84 % for TiO_2-CaH_2-350,
TiO_2-CaH_2-550 and TiO_2-CaH_2-850, respectively. Howe-
ver, there was a significant decrease in the MO degra-
dation rate constant as the initial dye concentration
increased above 10 ppm within 60 min of irradiation. This
decrease in rate constant with the increase

in MO dye concentration has several reasons. For
example, the increase in the initial MO dye concentrations
means more dye molecules are adsorbed on the TiO_2
catalyst surface. Therefore, a large amount of UV radia-
tion is absorbed by the MO dye molecules rather than by
the TiO_2 catalyst and hence, a decrease in the light pene-
trating to the surface of the TiO_2 catalyst is observed.[32] As
the active sites were occupied by more MO dye
molecules, the generation of reactive hydroxyl radicals
decreased.[33] Since the amount of catalyst and irradiation
time are constant, the formation of OH radicals upon the
surface of TiO_2 is also constant. So, with the increase in
MO dye concentration the surface requirements of catalyst
for the degradation process increases and therefore the
relative number of free radicals, which attack dye mo-
lecules, decreases.[34]

Table 8. Rates constants at different MO concentrations

Conc. of MO (ppm)	TiO$_2$-CaH$_2$-550		TiO$_2$-CaH$_2$-350		TiO$_2$-CaH$_2$-850	
	K (min^{-1})	Deg. %	K (min^{-1})	Deg. %	K (min^{-1})	Deg. %
5	0.0342	91	0.0241	81	0.0154	64
10	0.0418	95	0.0273	85	0.0264	84
15	0.0303	88	0.0221	78	0.0234	80
20	0.0227	79	0.0174	69	0.0209	76
25	0.017	68	0.014	60	0.0198	74
30	0.0124	55	0.0103	47	0.0174	69
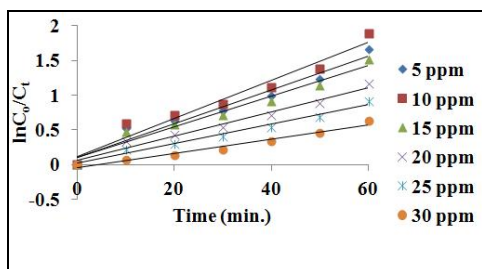
Fig. 16. Plot of ln (C_o/C_t) *vs.* reaction time at different initial concentrations of MO (TiO$_2$-CaH$_2$-350 = 40 mg, pH 4.5)
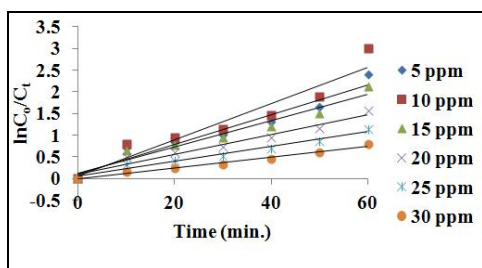
Fig. 17. Plot of ln (C_o/C_t) *vs.* reaction time at different initial concentrations of MO (TiO$_2$-CaH$_2$-550 = 40 mg, pH 4.5)
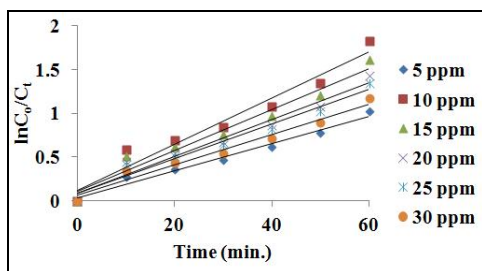
Fig. 18. Plot of ln (C_o/C_t) *vs.* reaction time at different initial concentrations of MO (TiO$_2$-CaH$_2$-850 = 40 mg, pH 4.5)

4. Conclusions

The aim of this work was to prepare reduced TiO$_2$ nanoparticles for the degradation of methyl orange dye with an activated visible light. Solid state reaction of TiO$_2$ with a reducing agent (CaH$_2$) in an inert argon atmosphere represents a facile approach to prepare reduced TiO$_2$. The crystalline phase of TiO$_2$ was not changed after the reduction reaction, while the crystalline size and lattice parameters were changed toward lower values as a result of the reduction treatment. The energy gap of TiO$_2$ showed a red shift that enhanced the absorption in the visible light region. Oxygen deficient oxides (TiO$_{2-x}$) formed as a result of the reduction conditions, were confirmed by the energy X-Ray dispersion spectroscopy. The reduced TiO$_2$ catalyst (TiO$_2$-CaH$_2$-550) showed excellent photocatalytic activity in the degradation of MO dye, with 95 % degradation.

Acknowledgements

References

[1] Li, Q.; Mahendra, S.; Lyon, D.Y.; Brunet, L.; Liga, M.V.; Li, D.; Alvarez, P.J.J. Antimicrobial Nanomaterials for Water Disinfection and Microbial Control: Potential Applications and Implications. *Water Res.* **2008**, *42*, 4591-4602. https://doi.org/10.1016/j.watres.2008.08.015

[2] Velichenko, A.; Knysh, V.; Luk'yanenko, T.V.; Dmitrikova, L.; Velichenko, Y.; Devilliers, D. PbO$_2$ Based Composite Materials Deposited from Suspension Electrolytes: Electrosynthesis, Physico-Chemical and Electrochemical Properties. *Chem. Chem. Technol.* **2012**, *6*, 123-133. https://doi.org/10.23939/chcht06.02.123

[3] Qu, X.; Alvarez, P.J.J.; Li, Q. Applications of Nanotechnology in Water and Wastewater Treatment. *Water Res.* **2013**, *47*, 3931-3946. https://doi.org/10.1016/j.watres.2012.09.058

[4] Wafiroh, S.; Abdulloh, A.; Widati, A.A. Cellulose Acetate Hollow Fiber Membranes from Banana Stem Fibers Coated by TiO$_2$ for Degradation of Waste Textile Dye. *Chem. Chem. Technol.* **2021**, *15*, 291-298. https://doi.org/10.23939/chcht15.02.291

[5] Maeda, K. Photocatalytic Water Splitting Using Semiconductor Particles: History and Recent Developments. *J. Photochem. Photobiol. C: Photochem. Rev.* **2011**, *12*, 237-268. https://doi.org/10.1016/j.jphotochemrev.2011.07.001

[6] Ameen, S.; Akhtar, M.S.; Seo, H.-K.; Shin, H.-S. Solution-Processed CeO$_2$/TiO$_2$ Nanocomposite as Potent Visible Light

Photocatalyst for the Degradation of Bromophenol Dye. *Chem. Eng. J.* **2014**, *247*, 193-198. https://doi.org/10.1016/j.cej.2014.02.104

[7] White, J.L.; Baruch, M.F.; Pander III, J.E.; Hu, Y.; Fortmeyer, I.C.; Park, J.E.; Zhang, T.; Liao, K.; Gu, J.; Yan, Y. *et al.* Light-Driven Heterogeneous Reduction of Carbon Dioxide: Photocatalysts and Photoelectrodes. *Chem. Rev.* **2015**, *115*, 12888-12935. https://doi.org/10.1021/acs.chemrev.5b00370

[8] Tahir, B.; Tahir, M.; Amin, N.A.S. Photo-Induced CO_2 Reduction by CH_4/H_2O to Fuels over Cu-Modified $g-C_3N_4$ Nanorods Under Simulated Solar Energy. *Appl. Surf. Sci.* **2017**, *419*, 875-885. https://doi.org/10.1016/j.apsusc.2017.05.117

[9] Malengreaux, C.M.; Pirard, S.L.; Léonard, G.; Mahy, J.G.; Herlitschke, M.; Klobes, B.; Hermann, R.; Heinrichs, B.; Bartlett, J.R. Study of the Photocatalytic Activity of Fe^{3+}, Cr^{3+}, La^{3+} and Eu^{3+} Single-Doped and co-Doped TiO_2 Catalysts Produced by Aqueous Sol-Gel Processing. *J. Alloys Compd.* **2017**, *691*, 726-738. https://doi.org/10.1016/j.jallcom.2016.08.211

[10] Lin, H.-Y.; Shih, C.-Y. Efficient One-Pot Microwave-Assisted Hydrothermal Synthesis of M (M= Cr, Ni, Cu, Nb) and Nitrogen co-Doped TiO_2 for Hydrogen Production by Photocatalytic Water Splitting. *J. Mol. Catal. A Chem.* **2016**, *411*, 128-137. https://doi.org/10.1016/j.molcata.2015.10.026

[11] Lei, J.; Chen, Y.; Shen, F.; Wang, L.; Liu, Y.; Zhang, J. Surface Modification of TiO_2 with $g-C_3N_4$ for Enhanced UV and Visible Photocatalytic Activity. *J. Alloys Compd.* **2015**, *631*, 328-334. https://doi.org/10.1016/j.jallcom.2015.01.080

[12] Kumar, S.G.; Rao, K.S.R.K. Comparison of Modification Strategies towards Enhanced Charge Carrier Separation and Photocatalytic Degradation Activity of Metal Oxide Semiconductors (TiO_2, WO_3 and ZnO). *Appl. Surf. Sci.* **2017**, *391*, 124-148. https://doi.org/10.1016/j.apsusc.2016.07.081

[13] Shi, J.; Chen, J.; Feng, Z.; Chen, T.; Lian, Y.; Wang, X.; Li, C. Photoluminescence Characteristics of TiO_2 and Their Relationship to the Photoassisted Reaction of Water/Methanol Mixture. *J. Phys. Chem. C* **2007**, *111*, 693-699. https://doi.org/10.1021/jp065744z

[14] Xia, T.; Zhang, Y.; Murowchick, J.; Chen, X. Vacuum-Treated Titanium Dioxide Nanocrystals: Optical Properties, Surface Disorder, Oxygen Vacancy, and Photocatalytic Activities. *Catal. Today* **2014**, *225*, 2-9. https://doi.org/10.1016/j.cattod.2013.08.026

[15] Lu, X.; Wang, G.; Zhai, T.; Yu, M.; Gan, J.; Tong, Y.; Li, Y. Hydrogenated TiO_2 Nanotube Arrays for Supercapacitors. *Nano Lett.* **2012**, *12*, 1690-1696. https://doi.org/10.1021/nl300173j

[16] Nikolenko, A.; Melnykov, B. Photocatalytic Oxidation of Formaldehyde Vapour Using Amorphous Titanium Dioxide. *Chem. Chem. Technol.* **2010**, *4*, 311-315. https://doi.org/10.23939/chcht04.04.311

[17] Yuan, Z.; Xiao-Xuan, W.; Lv, H.; Zheng, W.-C. EPR Parameters and Defect Structures of the off-Center Ti^{3+} Ion on the Sr^{2+} Site in Neutron-Irradiated $SrTiO_3$ Crystal. *J. Phys. Chem. Solids* **2007**, *68*, 1652-1655. https://doi.org/10.1016/j.jpcs.2007.04.001

[18] Bityurin, N.; Kuznetsov, A.I.; Kanaev, A. Kinetics of UV-Induced Darkening of Titanium-Oxide Gels. *Appl. Surf. Sci.* **2005**, *248*, 86-90. https://doi.org/10.1016/j.apsusc.2005.03.083

[19] Jenkins, C.A.; Murphy, D.M. Thermal and Photoreactivity of TiO_2 at the Gas–Solid Interface with Aliphatic and Aromatic Aldehydes. *J. Phys. Chem. B* **1999**, *103*, 1019-1026. https://doi.org/10.1021/jp982690n

[20] Coronel, S.; Pauker, C.S.; Jentzsch, P.V.; de la Torre, E.; Endara, D.; Muñoz-Bisesti, F. Titanium Dioxide/Copper/Carbon Composites for the Photocatalytic Degradation of Phenol. *Chem. Chem. Technol.* **2020**, *14*, 161-168. https://doi.org/10.23939/chcht14.02.161

[21] Qiu, S.; Kalita, S.J. Synthesis, Processing and Characterization of Nanocrystalline Titanium Dioxide. *Mater. Sci. Eng. A* **2006**, *435-436*, 327-332. https://doi.org/10.1016/j.msea.2006.07.062

[22] Liu, N.; Häublein, V.; Zhou, X.; Venkatesan, U.; Hartmann, M.; Mačković, M.; Nakajima, T.; Spiecker, E.; Osvet, A.; Frey, L.; Schmuki, P. "Black" TiO_2 Nanotubes Formed by High-Energy Proton Implantation Show Noble-Metal-co-Catalyst Free Photocatalytic H_2-Evolution. *Nano Lett.* **2015**, *15*, 6815-6820. https://doi.org/10.1021/acs.nanolett.5b02663

[23] Ullattil, S.G.; Periyat, P. A 'One Pot'Gel Combustion Strategy towards Ti^{3+} Self-Doped 'Black'Anatase TiO_{2-x} Solar Photocatalyst. *J. Mater. Chem. A* **2016**, *4*, 5854-5858. https://doi.org/10.1039/C6TA01993E

[24] Moore, D.M.; Reynolds, R.C., Jr. *X-Ray Diffraction and the Identification and Analysis of Clay Minerals*; Oxford university press: Oxford, 1989.

[25] Kulkarni, M.; Thakur, P. The Effect of $UV/TiO_2/H_2O_2$ Process and Influence of Operational Parameters on Photocatalytic Degradation of Azo Dye in Aqueous TiO_2 Suspension. *Chem. Chem. Technol.* **2010**, *4*, 265-270. https://doi.org/10.23939/chcht04.04.265

[26] Chen, Y.; Huang, W.; He, D.; Situ, Y.; Huang, H. Construction of Heterostructured $g-C_3N_4/Ag/TiO_2$ Microspheres with Enhanced Photocatalysis Performance under Visible-Light Irradiation. *ACS Appl. Mater. Interfaces* **2014**, *6*, 14405-14414. https://doi.org/10.1021/am503674e

[27] Wang, Z.; Yang, C.; Lin, T.; Yin, H.; Chen, P.; Wan, D.; Xu, F.; Huang, F.; Lin, J.; Xie, X. *et al.* Visible-Light Photocatalytic, Solar Thermal and Photoelectrochemical Properties of Aluminium-Reduced Black Titania. *Energy Environ. Sci.* **2013**, *6*, 3007-3014. https://doi.org/10.1039/C3EE41817K

[28] Amano, F.; Nakata, M.; Yamamoto, A.; Tanaka, T. Effect of Ti^{3+} Ions and Conduction Band Electrons on Photocatalytic and Photoelectrochemical Activity of Rutile Titania for Water Oxidation. *J. Phys. Chem. C* **2016**, *120*, 6467-6474. https://doi.org/10.1021/acs.jpcc.6b01481

[29] Zheng, J.; Liu, L.; Ji, G.; Yang, Q.; Zheng, L.; Zhang, J. Hydrogenated Anatase TiO_2 as Lithium-Ion Battery Anode: Size–Reactivity Correlation. *ACS Appl. Mater. Interfaces* **2016**, *8*, 20074-20081. https://doi.org/10.1021/acsami.6b05993

[30] Schwarzbauer, J.; Heim, S. Lipophilic Organic Contaminants in the Rhine River, Germany. *Water Res.* **2005**, *39*, 4735-4748. https://doi.org/10.1016/j.watres.2005.09.029

[31] Parveen, B. Room-Temperature Ferromagnetism in Ni-doped TiO_2 Diluted Magnetic Semiconductor Thin Films. *J. Appl. Res. Technol.* **2019**, *15*, 132-139. https://doi.org/10.1016/j.jart.2017.01.009

[32] Huang, X.; Han, S.; Huang, W.; Liu, X. Enhancing Solar Cell Efficiency: the Search for Luminescent Materials as Spectral Converters. *Chem. Soc. Rev.* **2013**, *42*, 173-201. https://doi.org/10.1039/C2CS35288E

[33] Qamar, M.; Muneer, M.; Bahnemann, D. Heterogeneous Photocatalysed Degradation of Two Selected Pesticide Derivatives, Triclopyr and Daminozid in Aqueous Suspensions of Titanium Dioxide. *J. Environ. Manage.* **2006**, *80*, 99-106. https://doi.org/10.1016/j.jenvman.2005.09.002

[34] Park, N.-G.; Van de Lagemaat, J.; Frank, A.J. Comparison of Dye-Sensitized Rutile- and Anatase-Based TiO_2 Solar Cells. *J. Phys. Chem. B* **2000**, *104*, 8989-8994. https://doi.org/10.1021/jp994365l

ФОТОКАТАЛІТИЧНА АКТИВНІСТЬ ДЕФЕКТНОГО TiO$_{2\text{-}x}$ ДЛЯ ОЧИЩЕННЯ ВОДИ/РОЗКЛАДУ БАРВНИКА МЕТИЛОВОГО ОРАНЖЕВОГО

Анотація. Метою цього дослідження є вивчення фотокаталітичної активності наночастинок TiO$_2$ в розкладі барвника метилового оранжевого (МО). Нанопорошок діоксиду титану TiO$_2$ був синтезований звичайним золь-гель методом і кальцинований в атмосфері повітря за різних температур (350℃, 550℃ і 850℃). Потім синтезовані наночастинки TiO$_2$ піддавали твердофазній реакції з Кальцій гідридом (CaH$_2$) за тих же температур в атмосфері аргону. Вимірювання рентгенівської дифракції (XRD), використані для ідентифікації фази та розміру кристалів, показали, що отримані зразки мають однакову фазу анатазу TiO$_2$, але розмір кристалів зменшився після відновлювальної обробки. Електронні властивості, отримані за допомогою УФ-спектроскопії, показали зменшення розрахованого енергетичного проміжку з 3,3 еВ для одержаного TiO$_2$-550 до 2,65 еВ для відновленого TiO$_2$-CaH$_2$-550, що розширює спектри поглинання до області видимого світла. Вимірювання за допомогою енергетичної дисперсійної спектроскопії (EDS) і сканувальної електронної мікроскопії (SEM) показали, що розмір частинок зменшується після відновлювальної обробки, подібно до XRD розміру кристалів. Результати EDS показали, що нестача вмісту Оксигену пов'язана з утворенням оксигенових вакансій, які є причиною утворення нестехіометричних оксидів TiO$_{2\text{-}x}$. Синтезований відновлений TiO$_2$ показав чудову фотокаталітичну активність у розкладі барвника метилового оранжевого за оптимальних умов: pH 4,5, завантаження каталізатора 40 мг і початкова концентрація барвника 10 м.ч.

Ключові слова: CaH$_2$, фотокаталітична активність, оксигенові вакансії, твердий стан, TiO$_2$.